Geothermal Modeling By Gauss-Legendre Quadrature Integration

Timothy E. Leftwich (tim.leftwich@dnr.state.oh.us)[1], Ralph R. B. von Frese (vonfrese@geology.ohio-state.edu)[2], and Brian Tost (tost.2@osu.edu)[2]

[1]Ohio Department of Natural Resources, Division of Geological Survey; [2]The Ohio State University

Abstract

Bottom-hole temperature data and temperature-dependent seismic, gravity, magnetic, and other geological data increasingly are becoming available for improving our understanding of the geological structure and evolution of Earth, aiding fossil energy exploration and CO_2 sequestration efforts as well as for enhancing geothermal-energy exploration. In assessing these growing data sets, there is a great need for developing methods to compute regional and local thermal fields from geologic models in spherical as well as Cartesian coordinates. We explore the utility of the elegant Gauss-Legendre quadrature formulation for numerically modeling the thermal effects (i.e., potential and field) of the spherical prism for heat productivity contrasts in radiogenic content and thermal conductivity. As an application, we investigate the potential (T) and heat flow (q) effects of real terrain on BHT observations and heat flow estimates in Ohio.

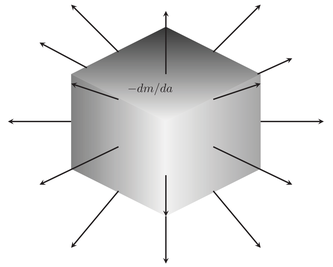

FIGURE 1.—Schematic positive heat production contrast element (da). The field lines emanate from the source/sink exactly like a density contrast $-dm$.

FIGURE 2.—The differential mass at $S(r_s,\theta_s,\Phi_s)$ produces a scalar potential U_{os} and the differential heat-producing source produces a scalar potential T_{os} at the observation point $O(r_o,\theta_o,\Phi_o)$.

$$dT_{os} = \frac{da_s}{4\pi\lambda R_{os}} \quad (1)$$

$$dq_{os} = \nabla(dT_{os}) = -\lambda\frac{\partial dT_{os}}{\partial R_{os}} = -\frac{da_s}{4\pi}\frac{\partial}{\partial R_{os}}\left(\frac{1}{R_{os}}\right) \quad (2)$$

Poisson's relation for sources with common density and heat productivity differentials; q is related to the gravity field, g, [*Simmons*, 1967] by:

$$q = g\frac{\mathbf{A}_s}{2\pi G\rho_s} \quad (3)$$

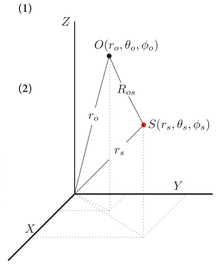

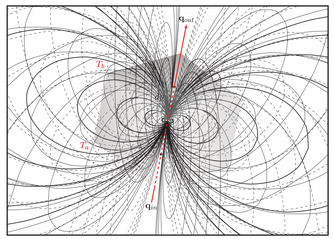

FIGURE 3.—Schematic cutaway positive thermal-conductivity contrast element (dp) oriented in the direction of the inducing flow of heat. Unlike a heat-producing element, a positive thermal-conductivity contrast reduces the potential (T) on the negative side and increases it on the positive side, yielding a field configuration that is exactly like an induced dipolar magnetic field [*Carslaw and Jaeger*, 1959; *Jaeger*, 1965]. The energy entering the element (in W) is q. The potential ($T_{ab} = T_a - T_b$) drop across the element is converted into work in the differential alteration of the T field. The field lines placed in the page plane are drawn as thick lines, the field lines in front of the page with thin solid lines, and those behind with dashed lines.

FIGURE 4.—The differential thermal-conductivity contrasting source at $S(r_s,\theta_s,\Phi_s)$ produces a scalar potential T_{os} at the observation point $O(r_o,\theta_o,\Phi_o)$. Like the magnetic moment vector, dp may be represented by its magnitude dp_s, declination D_s and inclination I_s or its vector components in Earth-centered cartesian ($dp_{xs}, dp_{ys}, dp_{zs}$) or spherical ($dp_s, r_s, dp_\theta, \Phi_s, dp_r, \Phi_s$) coordinate systems.

The magnetic potential is

$$dW_{os} = -\frac{\mu_o}{4\pi}\frac{\cos\alpha}{R_{os}^2}dj_s \quad (4)$$

and the thermal potential T by

$$dT_{os} = -\frac{1}{4\pi\lambda}\frac{\cos\alpha}{R_{os}^2}dp_s \quad (5)$$

By Poisson's relation for sources with common density, ρ, and heat capacity, c, differentials, the potential, T, is proportional to the component of gravity in the direction of polarization, ζ, by

$$T = -\frac{\mathbf{P}_s}{G\rho\lambda}\left(\frac{\partial U}{\partial\zeta}\right) \quad (6)$$

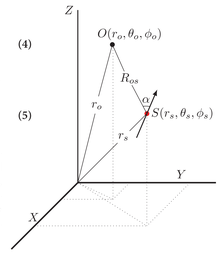

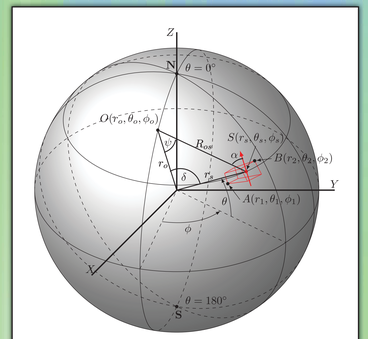

FIGURE 5.—Spherical geometry for modeling at the observation point $O(r_o,\theta_o,\Phi_o)$ the thermal effects of the spherical prism by integrating the unit source (e.g., $dj_s = A_s dV$ for a heat-producing source or $dp_s = \mathbf{P}_s dV$ for a thermal-conductivity contrast) through the volume of the prism with bottom and top surfaces that include the representative corner points $A(r_1,\theta_1,\Phi_1)$ and $B(r_2,\theta_2,\Phi_2)$, respectively. The Cartesian perspective is given by the superposed, co-registered X, Y, and Z axes.

For heat productivity then, T is given by

$$T_{os} = \int_V dT_{os} = \frac{1}{4\pi\lambda}\int_V \frac{1}{R_{os}}\mathbf{A}_s dV \quad (7)$$

and the heat flow anomaly is

$$q_{os} = \int_V dq_{os} = \frac{1}{4\pi\lambda}\int_V \frac{1}{R_{os}}\mathbf{A}_s dV \quad (8)$$

For a thermal-conductivity contrast, T is

$$T_{os} = \int_V dT_{os} = -\frac{1}{4\pi\lambda}\int_V \frac{\cos\alpha}{R_{os}^2}\mathbf{P}_s dV \quad (9)$$

and the heat flow anomaly is

$$q_{os} = \int_V dq_{os} = -\frac{1}{4\pi\lambda}\int_V \Delta\left(\frac{\cos\alpha}{R_{os}^2}\right)\mathbf{P}_s dV \quad (10)$$

For the unit volume with $c_i\rho_i$ in homogeneous media with $c_2\rho_2$:

$$\mathbf{P}_s = -q\left(\frac{1}{c_1\rho_1} - \frac{1}{c_2\rho_2}\right)c_1\rho_1 = -q\left(1 - \frac{c_1\rho_1}{c_2\rho_2}\right) \quad (11)$$

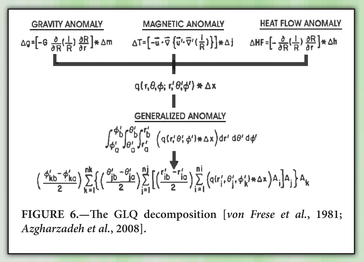

FIGURE 6.—The GLQ decomposition [*von Frese et al.*, 1981; *Azgharzadeh et al.*, 2008].

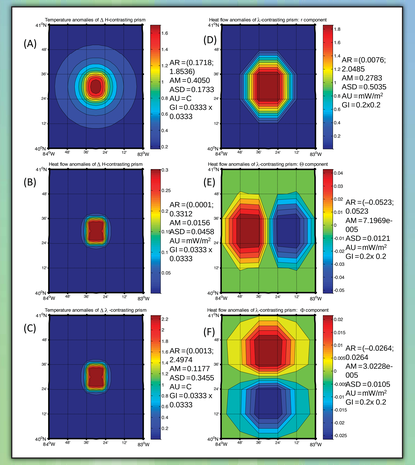

FIGURE7.—Temperature and heat flow anomalies associated with 0.2°×0.2°×1km crustal prism. For heat production, we assumed $A_s = 1\times10^{-6}$Wm^{-3} to estimate the temperature (A) and heat flow (B) effects. The temperature anomalies from the thermal-conductivity contrasting prism (C) were also modeled. The radical q_r, E–W (q_θ), and N–S (q_ϕ) heat flow anomalies from the thermal-conductivity contrasting prism are shown in (D), (E), and (F), respectively. We assumed $I = -90°$, $D = 0°$, thermal susceptibility = 0.03, and nominal heat flow $q = 0.05$ Wm^{-3}. These effects are for the infinite medium case and, unlike gravity and magnetism, are doubled at Earth's surface boundary.

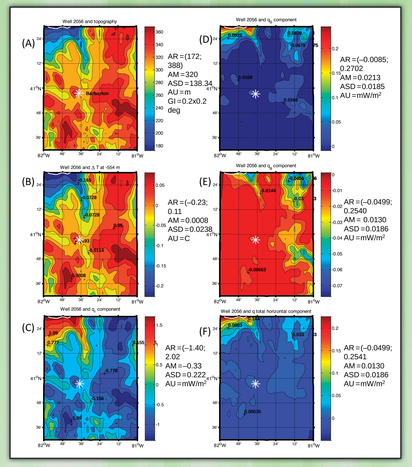

FIGURE 10.—(A) Topography with location of well 2056 in Summit County with (B) terrain temperature effects at bottom-hole depth (–554 m), (C) q_r, (D) q_θ, (E) q_φ, and (F) total horizontal heat flow anomalies.

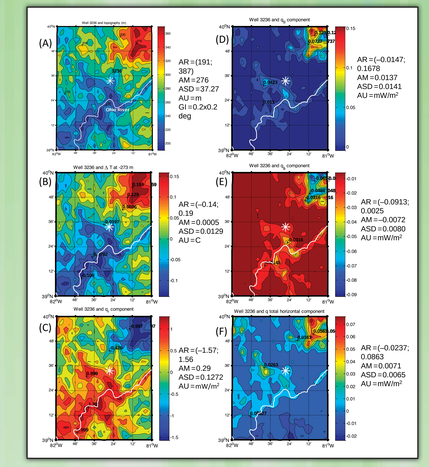

FIGURE 11.—(A) Topography with location of well 3236 in Washington County, Ohio with (B) terrain temperature effects at bottom-hole depth (–273 m), (C) q_r, (D) q_θ, (E) q_φ, and (F) total horizontal heat flow anomalies.

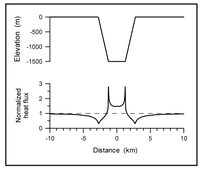

FIGURE 8.—Terrain has strong thermal effects. Normalized topographic heat flow effects from the plane-slope calculation [*Lachenbruch*, 1968; *Van der Veen et al.*, 2007] for a valley with a depth-to-width ratio of 2:1.

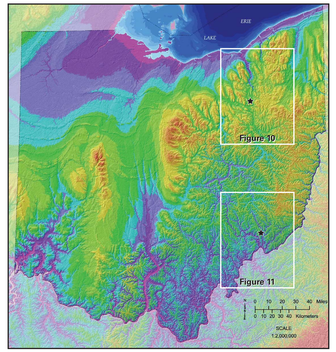

FIGURE 9.—Location of Ohio heat flow estimates [*Eckstein et al.*, 1982] on spectral topography [*Ohio Division of Geological Survey*, 2002].

Conclusions

- Poisson's relation allows Laplacian computation of steady thermal fields.
- GLQ integrations for arbitrary heat production and Δλ sources (e.g., terrain).
- The GLQ correction (Figure 10.D) at well 2056 in Summit County is –0.46 mWm^{-2}, and the GLQ correction (Figure 11.D) at well 3236 in Washington County is 0.714 mWm^{-2}.
- The GLQ-corrected heat flow value at well 2056 is 58.24 mWm^{-2}, and the GLQ-corrected heat flow value at well 3236 is 54.93 mWm^{-2}.

References

Asgharzadeh, M. F., R. R. B. von Frese, H. R. Kim (2008), Spherical prism magnetic effects by Gauss-Legendre quadrature integration, *Geophys. J. Int.*, *173*, 315–333, doi:10.1111/j.1365-246X.2007.03692.x.

Carslaw, H. S., and J. C. Jaeger (1959), *Conduction of Heat in Solids*, 510 pp., Oxford Univ. Press, London.

Eckstein, Y., R. A. Heimlich, D. F. Palmer, S. S. Shannon, Jr. (1982), Geothermal investigations in Ohio and Pennsylvania, rep. LA-9223-HDR, 89 pp., Los Alamos Nat. Lab., Los Alamos, N. M.

Jaeger, J. C. (1965), Application of the theory of heat conduction to geothermal measurements, in *Terrestrial Heat Flow*, *Geophys. Monogr. Ser.*, vol. 8, edited by W. H. K. Lee, pp. 7–23, AGU, Washington, D. C.

Lachenbruch, A. H. (1968), Estimation of the topographic disturbance to superficial thermal gradients, *Rev. Geophys.*, *6*, 365–400.

Ohio Division of Geological Survey (2002), Shaded elevation map of Ohio, spectral version, Map MG-1 page-size, Ohio Dept. of Natural Resources, Div. of Geological Survey, Columbus, Oh.

Simmons, G. (1967), Interpretations of heat flow anomalies, *Rev. Geophys.*, *5*, 43–52.

Van der Veen, C. J., T. E. Leftwich, R. R. B. von Frese, B. Csatho, and R. Li (2007), Subglacial topography and geothermal heat flux: Potential interactions with drainage of the Greenland Ice Sheet, *Geophys. Res. Lett.*, *34*, L12501, 5 pp., doi: 10.1029/2007GL030046.

von Frese, R. R. B., W. J. Hinze, L. W. Braile, and A. J. Luca (1981), Spherical Earth gravity and magnetic anomaly modeling by Gauss-Legendre quadrature integration, *J. Geopyhys.*, *49*, 234–242.

AASG Association of American State Geologists

IN33C-1475